Identification of Time-varying Parameters of a Monthly Budyko Function and its Implications

Weibo Liu [a, b, c], Pan Liu [a, b, c *], Lei Cheng [a, b, c], Xiaojing Zhang [a, b, c], Liting Zhou [a, b, c]

[a] State Key Laboratory of Water Resources and Hydropower Engineering Science, Wuhan University, Wuhan 430072, China

[b] Hubei Provincial Key Lab of Water System Science for Sponge City Construction, Wuhan University, Wuhan 430072, China

[c] Research Institute for Water Security (RIWS), Wuhan University, Wuhan 430072, China.

[*]Correspondence to: Pan Liu liupan@whu.edu.cn

Abstract: The Budyko framework, which can describe a simple but useful partitioning of precipitation under supply and energy limits, is used widely to estimate evapotranspiration (*ET*). Previous studies have investigated time-variant Budyko functions on annual or interannual scales but seldom on the intra-annual scale. This study used a monthly two-parameter (κ and y_0) Budyko function and three schemes that considered single observations (*ET* or streamflow (*Q*)) and dual observations (*ET* and *Q*) to assimilate the time-varying parameters using the ensemble Kalman filter method. The study considered the contiguous USA (CONUS) using the Model Parameter Estimation Experiment dataset. The time-varying parameters were explained on the basis of time series analysis and correlation with meteorological data. Three conclusions were as follows. (1) The identified time-varying parameters (κ and y_0) of the Budyko function could effectively simulate *ET*. (2) The assimilation using only *ET* observations could identify a plausible set for parameter κ but was inadequate for y_0. (3) Most time-varying parameters exhibited a 12-month period, and the trend and change points detected for Midwest CONUS were related to anthropogenic influences such as extraction and use of groundwater. The findings show that changing environment can be detected by using the proposed time-varying parameters of the Budyko function.
Keywords: monthly Budyko function; time-varying parameters; ensemble Kalman filter; contiguous USA; MOPEX dataset;

1. Introduction

Hydrological models generalize the complex processes of the water cycle, which is of great importance in relation to research and experiments on the hydrological system. Parameters adopted in hydrological models play a crucial role in simulation performance and are often calibrated as constants. However, as with the effects of varying conditions such as afforestation, climate change, and human activities (Peel & Bloschl, 2011; Wu & Johnston, 2007), model parameters cannot be treated as time-invariant. Thus, it is more practical to analyze model parameters taking time-variant climatic factors and underlying surface conditions into consideration (Merz, Parajka,

& Bloschl, 2011; Patil & Stieglitz, 2015; Thirel et al., 2015).

The responses of time-varying parameters to changes in the underlying surface and climatic conditions can be obtained using various methods. For example, the functional form of parameters can be established with seasonal, annual, or interannual trends (Jeremiah, Marshall, Sisson, & Sharma, 2013; Marshall, Sharma, & Nott, 2006; Westra, Thyer, Leonard, Kavetski, & Lambert, 2014). However, additional judgement is required to establish such functions and the parameters must always be adjusted for different situations. An alternative method is to calibrate the model parameters by dividing the available data into consecutive subsets using optimization algorithms (de Vos, Rientjes, & Gupta, 2010; Seibert, McDonnell, & Woodsmith, 2010; Vaze et al., 2010). Unfortunately, the selection of such subsets is subjective, and optimization algorithms based on simple screening criteria (commonly, the Nash–Sutcliffe efficiency (NSE) for runoff) cannot take full advantage of the information provided by climatic data.

The data assimilation (DA) technique, the main concept of which is to compare the errors between observations and model simulations to obtain optimal estimates of the current system, is used widely to identify model parameters. Through the balance of information (uncertainties) between a model and observations, the observations can be used via DA to update model states and obtain model parameters simultaneously (Abbaszadeh, Moradkhani, & Yan, 2018; Clark et al., 2008). In studies that focus on identifying parameters, application of DA methods is generally effective (Chao Deng, Liu, Guo, Li, & Wang, 2016; Feng et al., 2017; Smith, Beven, & Tawn, 2008; Vrugt, ter Braak, Diks, & Schoups, 2013). Additionally, more than one set of observations could be used to improve the efficiency of the DA method (M. S. Xiong et al., 2019). However, similar to traditional optimization algorithms, DA methods have problems regarding parameter equifinality when the hydrological model has a number of parameters. To overcome this drawback, a simple model such as the Budyko framework was used in this study.

The Budyko framework contains few parameters, and describes a simple but useful partitioning of precipitation into evaporation and runoff under supply and energy limits (Sankarasubramanian. et al., 2020). The Budyko hypothesis is that

multiyear average evaporation depends on available water capacity and atmospheric water requirement. The framework based on the Budyko hypothesis has been used extensively in the hydrological field to estimate evaporation (Bagrov, 1953; Fu, 1981; Mezentsev, 1955; Milly, 1994; Pike, 1964; Porporato, Daly, & Rodriguez-Iturbe, 2004; Turc, 1954; Yang et al., 2007; L. Zhang, Dawes, & Walker, 2001; L. Zhang et al., 2004).

Budyko-type equations have been applied widely on annual or interannual scales, and time-varying investigations at such temporal scales have recently drawn considerable attention. For example, Sinha, Jha, and Goyal (2019) estimated mean annual-scale watershed parameter with watershed properties using the multiple linear regression method and machine learning techniques. X. Zhang, Dong, Cheng, and Xia (2019) improved the fitting capability for most catchments in the United States by establishing a function between annual-scale time-varying parameters and time steps. However, few studies have focused on the time-varying parameters of Budyko functions at the intra-annual (e.g., monthly) scale. Model parameters on long temporal scales represent an average reflection of the annual or interannual climatic and underlying conditions, and their variation weakens at such scales. Consequently, important change rules regarding both parameters and varying climatic conditions might not be investigated adequately on annual or interannual scales. Moreover, assumptions and applicability might lead to deviations when the Budyko framework is applied on shorter temporal scales (Mianabadi, Davary, Pourreza-Bilondi, & Coenders-Gerrits, 2020). For example, to investigate time-variant conditions using the Budyko equation, soil water content must be changeable on the intra-annual scale, which is markedly different to that on the annual scale.

Thus, this study investigated time-varying Budyko functions on the intra-annual scale. The main objectives of this research were as follows: (1) to investigate an effective approach for identification of intra-annual-scale time-varying parameters of the Budyko function, (2) to determine whether evaporation observations alone or in combination with streamflow observations could be used effectively to assimilate parameters, and (3) to establish whether reasonable change rules regarding parameters could be explained on the basis of the climatic or underlying conditions. The remainder of this paper is organized as follows. The methods and experimental design

are introduced in Section 2. Section 3 describes the case study, including the study area and parameter setting. The results are presented and discussed in Section 4. Finally, our conclusions are stated in Section 5.

2. Methodology

An overview of the methods and analysis structure adopted for this study are shown in **Fig. 1**. Three schemes that considered single observations (*ET* or streamflow (*Q*)) and dual observations (*ET* and *Q*) were used to incorporate different observations into the assimilation. Subsequently, parameter sets were analyzed through time series analysis.

2.1 A two-parameter Budyko function for evaporation calculation

Greve, Gudmundsson, Orlowsky, and Seneviratne (2016) proposed a two-parameter Budyko function that can be used for the intra-annual dimension, e.g., the monthly scale. The parameters of this equation are κ and y_0, which constitute the following equation:

$$\frac{E}{P} = F\left(\Phi, \kappa, y_0\right) = 1 + \Phi - \left(1 + \left(1 - y_0\right)^{\kappa - 1} \left(\Phi\right)^{\kappa}\right)^{\frac{1}{\kappa}} \quad (1)$$

where E is the evaporation of the catchment, P represents precipitation, and Φ is the aridity index (*AI*), which is calculated as the ratio of potential evaporation and precipitation.

As in the traditional Budyko approach, the first parameter κ is a free model parameter, while the second parameter y_0 has physical significance because it might account for the maximum amount of additional water available to E (Greve et al., 2016). Specifically, Greve et al. (2016) interpret κ as the integrator of various factors other than the *AI* that influence the partitioning of precipitation. It can have wide application in relation to monthly data and is suitable for conditions when

evapotranspiration exceeds precipitation from the monthly to annual scale.

2.2 Calculation of monthly runoff

Monthly runoff can be calculated to assimilate runoff observations. Generally, runoff is connected with soil moisture on the monthly scale, and runoff can be assumed to have a hyperbolic tangent relationship with soil water content (L. H. Xiong & Guo, 1999), which can be expressed as follows:

$$Q_t = S_t \times \tanh(S_t / SC) \tag{2}$$

where Q_t is the monthly streamflow and S_t represents the soil water content, which is the specific parameter that can reflect the water storage capacity (SC) of the watershed.

Finally, the monthly soil water content can be expressed as follows:

$$S_t = S_{t-1} + P_t - ET_t - Q_t \tag{3}$$

Descriptions and ranges of the parameters introduced in Section 2.1 and 2.2, listed in **Table** , are based on previous research by M. S. Xiong et al. (2019) and Greve et al. (2016).

2.3 Ensemble Kalman filter

The ensemble Kalman filter (EnKF) is a type of DA technique that uses sequential data, in which an error covariance matrix is approximated using the Monte-Carlo method. An ensemble of state simulations is generated to regenerate the state variables and calibrate the model parameters, i.e., update is performed on the basis of a sequence of observed data (C. Deng, Liu, Guo, Wang, & Wang, 2015; Evensen, 1994). The steps necessary in application of the EnKF method are as follows.

(1) Initialize the background field. First, choose the state and observation variables to build the equations. Second, set the size of ensemble N and the length of the time step n for the DA, which is determined by the data length. Then, the state variables are created following a Gaussian distribution.

(2) Forecast the value. After initializing the background field at time step k, forecasts of state variables and model parameters can be generated by disturbing the values updated from the previous time step. The state equation is as follows:

$$\begin{pmatrix} \theta_{i,k+1}^{f} \\ x_{i,k+1}^{f} \end{pmatrix} = \begin{pmatrix} \theta_{i,k}^{a} \\ f(x_{i,k}^{a}, \theta_{i,k+1}^{f}) \end{pmatrix} + \begin{pmatrix} \delta_{i,k} \\ \varepsilon_{i,k} \end{pmatrix}, \ \delta_{i,k} \sim N(0, R_k), \varepsilon_{i,k} \sim N(0, G_k) \tag{4}$$

where $\theta_{i,k+1}^{f}$ (parameter vector) and $x_{i,k+1}^{f}$ (state vector) mean the i-th ensemble forecast variable at time step $k+1$; $\theta_{i,k}^{a}$ and $x_{i,k}^{a}$ are analysis variables of the i-th ensemble member at time step k; f can be described as a model operator; and $\delta_{i,k}$ and $\varepsilon_{i,k}$ represent the model error (white noise) of the i-th ensemble member. It should be noted that the model errors obey a normal distribution with mean value of zero and variance (R_k, G_k). All uncertainties regarding the model structure and data are reflected in $\varepsilon_{i,k}$.

(3) Observation perturbing. The universal observation equation is as follows:

$$y_{i,k+1} = h(x_{k+1}, \theta_{k+1}) + \xi_{i,k+1}, \xi_{i,k+1} \sim N(0, S_k) \tag{5}$$

where $y_{i,k+1}$ is the simulation value of the i-th ensemble member at time step $k+1$; y_{k+1} is the observation vector of time $k+1$; h is the observational operator that converts the model state variables to observations; and $\xi_{i,k+1}$ is the measurement error following the normal distribution.

(4) Update. The updating process is formalized as follows:

$$\begin{pmatrix} \theta_{i,k+1}^{a} \\ x_{i,k+1}^{a} \end{pmatrix} = \begin{pmatrix} \theta_{i,k+1}^{f} \\ x_{i,k+1}^{f} \end{pmatrix} + \begin{pmatrix} K_{k+1}^{\theta}[y_{i,k+1} - h(x_{i,k+1}^{f}, \theta_{i,k+1}^{f})] \\ K_{k+1}^{x}[y_{i,k+1} - h(x_{i,k+1}^{f}, \theta_{i,k+1}^{f})] \end{pmatrix} \tag{6}$$

where K_{k+1} represents the Kalman gain matrix, the calculation method of which was described by Moradkhani, Sorooshian, Gupta, and Houser (2005) as follows:

$$K_{k+1}^{x} = \sum_{k+1}^{xy} \left(\sum_{k+1}^{yy} + S_k \right)^{-1}, \quad K_{k+1}^{\theta} = \sum_{k+1}^{\theta y} \left(\sum_{k+1}^{yy} + S_k \right)^{-1} \tag{7}$$

$$\sum_{k+1}^{xy} = \frac{1}{N-1} \sum_{i=1}^{N} (x_{i,k+1}^{f} - \bar{x}_{k+1}^{f})(\hat{y}_{i,k+1} - \hat{y}_{i,k+1}^{m})^{T} \tag{8}$$

$$\sum_{k+1}^{\theta y} = \frac{1}{N-1} \sum_{i=1}^{N} (\theta_{i,k+1}^{f} - \bar{\theta}_{k+1}^{f})(\hat{y}_{i,k+1} - \hat{y}_{i,k+1}^{m})^{T} \tag{9}$$

$$\sum_{k+1}^{yy} = \frac{1}{N-1} \sum_{i=1}^{N} (\hat{y}_{i,k+1} - \hat{y}_{i,k+1}^{m})(\hat{y}_{i,k+1} - \hat{y}_{i,k+1}^{m})^{T} \tag{10}$$

where $\sum_{k+1}^{xy}$ is the cross covariance of the simulated $\hat{y}_{i,k+1}$ and forecasted states $x_{i,k+1}^{f}$ (Snyder & Zhang, 2003); $\sum_{k+1}^{\theta y}$ is the cross covariance of the simulated $\hat{y}_{i,k+1}$ and forecasted parameters; $\sum_{k+1}^{yy}$ represents the error covariance of the simulated $\hat{y}_{i,k+1}$ (Mitchell & Houtekamer, 2000); $\bar{x}_{k+1}^{f}$ and $\bar{\theta}_{k+1}^{f}$ are the means of the forecasted states and parameter ensembles, respectively; and $\hat{y}_{i,k+1}^{m}$ is the mean of the simulated $\hat{y}_{i,k+1}$ ensemble.

2.4 Experimental design

Using the evaporation and runoff calculation, the state and observation equations can be described as follows:

State equation:

193
$$\begin{pmatrix} \kappa_{1,k+1}^{f} \\ y_{01,k+1}^{f} \end{pmatrix} = \begin{pmatrix} \kappa_{1,k}^{a} \\ y_{01,k}^{a} \end{pmatrix} + \begin{pmatrix} \delta_{1,1,k} \\ \delta_{2,1,k} \end{pmatrix} \quad (11)$$

194
$$\begin{pmatrix} \kappa_{1,k+1}^{f} \\ y_{01,k+1}^{f} \\ SC_{1,k+1}^{f} \\ S_{1,k+1}^{f} \end{pmatrix} = \begin{pmatrix} \kappa_{1,k}^{a} \\ y_{01,k}^{a} \\ SC_{1,k}^{a} \\ f(S_{1,k}^{a}, \kappa_{1,k+1}^{f}, y_{01,k+1}^{f}, SC_{1,k+1}^{f}) \end{pmatrix} + \begin{pmatrix} \delta_{1,1,k} \\ \delta_{2,1,k} \\ \delta_{3,1,k} \\ \varepsilon_{1,k} \end{pmatrix} \quad (12)$$

195 Observation equation:

196
$$ET_{k+1} = h(\kappa_{k+1}^{f}, y_{0k+1}^{f}) + \xi_{1,k+1} \quad (13)$$

197
$$Q_{k+1} = h(S_{k+1}^{f}, \kappa_{k+1}^{f}, y_{0k+1}^{f}, SC_{k+1}^{f}) + \xi_{2,k+1} \quad (14)$$

198
$$\begin{pmatrix} ET_{k+1} \\ Q_{k+1} \end{pmatrix} = \begin{pmatrix} h(\kappa_{k+1}^{f}, y_{0k+1}^{f}) \\ h(S_{k+1}^{f}, \kappa_{k+1}^{f}, y_{0k+1}^{f}, SC_{k+1}^{f}) \end{pmatrix} + \begin{pmatrix} \xi_{1,k+1} \\ \xi_{2,k+1} \end{pmatrix} \quad (15)$$

199 Three schemes were designed to obtain time-varying hydrological model
200 parameters by the DA method using single data (*ET* or *Q*) and multivariate data (*ET*
201 and *Q*). Experimental investigation was implemented to compare the three schemes in
202 terms of model efficiency and parameter variation. Each of the three schemes is
203 outlined below and brief descriptions are presented in Table 2. Descriptions of the
204 assimilated time-varying parameters, calculation modules and observational data of
205 the designed experimental schemes.

206 (1) Scheme 1 updates model parameters κ and y_0 by assimilating only ET data
207 with the two-parameter Budyko function to investigate the performance of
208 assimilation through the simple equation. Owing to the low complexity, there is no
209 state variable in this scheme. Thus, Eqs. (11) and (13) are included in Scheme 1.

210 (2) Scheme 2 assimilates only Q data to update the model parameters. The
211 difference from Scheme 1 is that the model combines the Budyko function with the
212 monthly water balance model and the number of parameters is increased to three: κ,
213 y_0, and SC. The state variable S is updated solely by assimilating Q. Therefore,

Scheme 2 contains Eqs. (12) and (14).

(3) Scheme 3 uses an additional set of data. Multivariate data are used to update both model parameters κ, y_0, and SC and state variable S. The model structure of Scheme 3 is similar to that of Scheme 2, in that both the Budyko function and the water balance model are used to obtain the parameters. Thus, Scheme 3 uses Eqs. (12) and (15).

2.5 Performance evaluation criteria

(1) The NSE (Nash & Sutcliffe, 1970) is an evaluation criterion applicable to evaluation of the effect of DA in this study:

$$NSE = 1 - \frac{\sum_{i=1}^{n} (y_{sim,i} - y_{obs,i})^2}{\sum_{i=1}^{n} (y_{sim,i} - \overline{y}_{obs})^2} \tag{16}$$

where $y_{sim,i}$ and $y_{obs,i}$ are the simulated and observed variables for the i-th month, respectively, $\overline{y}_{obs}$ is the average of the observed variable, and n is the total number of data time points. The NSE value ranges from $-\infty$ to 1, where the upper limit means perfect match between the simulation and observations.

(2) Kling–Gupta efficiency (KGE) is implemented through three components to avoid the NSE sensitivity to the data peak:

$$KGE = 1 - \sqrt{(r-1)^2 + (\frac{\sigma_{sim}}{\sigma_{obs}} - 1)^2 + (\frac{\mu_{sim}}{\mu_{obs}} - 1)^2} \tag{17}$$

where r is the correlation coefficient of the simulated and observed data, and σ_{sim}, σ_{obs}, μ_{sim}, and μ_{obs} are the standard deviations and mean values of the simulated and observed data, respectively.

(3) The Pearson correlation coefficient (R) was used to detect linear relationships between the assimilated parameters and between the parameters and the

meteorological factors:

$$R = \frac{\sum_{i=1}^{n}(a-\bar{a})(b-\bar{b})}{\sqrt{\sum_{i=1}^{n}(a-\bar{a})^2(b-\bar{b})^2}} \quad (18)$$

where a and b represent the correlated variables, and $\bar{a}$ and $\bar{b}$ represent the mean values of the variables.

(4) The root mean square error (RMSE) and volume error (VE), which were used to evaluate the estimated parameter results in our study, reflect the differences between simulated and observed variables:

$$RMSE=\sqrt{\frac{1}{n}\sum_{i=1}^{n}(y_{sim,i}-y_{obs,i})^2} \quad (19)$$

$$VE = \frac{\sum_{i=1}^{n} y_{sim,i} - \sum_{i=1}^{n} y_{obs,i}}{\sum_{i=1}^{n} y_{obs,i}} \quad (20)$$

where $y_{sim,i}$ and $y_{obs,i}$ are the simulated and observed variables, respectively.

(5) Diversity (defined just like the mean absolute relative error) is used to measure differences between the absolute values of two sets of data:

$$D = \frac{1}{n}\sum_{i=1}^{n}\frac{\left|x_{\exp,i}-x_{ref,i}\right|}{x_{ref,i}} \quad (21)$$

where $x_{\exp,i}$ and $x_{ref,i}$ are the experimental and reference values, respectively.

2.6 Time series analytical methods

Three time series analytical methods were used to detect the trend, change points, and periodicity of the parameters to elucidate potential variation rules.

(1) The Mann–Kendall trend test method (Kendall, 1975; Mann, 1945) has been used widely for detecting data trends and is recommended as a standard method by the World Meteorological Organization (Ziegler et al., 2003). If the standard normal statistical variables are positive, there is an upward trend in the time series data, and vice versa.

(2) The Pettitt test is a nonparametric approach that was first used to examine the change point of a dataset by Pettitt (1979). This method is simple and appropriate for identifying the change points of data and parameters. Thus, we applied this method to analyze the change points in this study.

(3) The wavelet transform analysis method, which can identify periodic changes by exploring the fluctuation signal law and distribution of multiple temporal scale hydrological sequences, has been used in general analysis of the laws of variation and periodicity of rainfall, runoff, and storage water (Shao Xiaomei, 2006). The function of the Morlet wavelet transform was used in this study to detect the periodicity of the parameters, because wavelet variance can reflect the principal period and other oscillation cycles of the parameters.

3. Case study

3.1 Study region and dataset

This study considered the contiguous USA (CONUS), which lies within the region 25°–49°N, 70°–130°W. The attributes of the studied catchments and relevant climatic data were obtained from the Model Parameter Estimation Experiment (MOPEX) (Duan et al., 2006). The hydrometeorological dataset extended between 1983 and 2003, in which precipitation and streamflow data were obtained from MOPEX, and potential evaporation and actual evaporation data were collected from a remote sensing dataset provided by the University of Montana (K. Zhang, Kimball, Nemani, & Running, 2010). In this dataset, actual evaporation is obtained using the Penman–Monteith equation (Monteith, 1972; Penman, 1948) and remote sensing results, and potential evaporation is computed using the Priestly–Taylor method (Priestley, 1972). To introduce data reflecting vegetation cover conditions, bimonthly

normalized difference vegetation index (*NDVI*) data were obtained from 8-km spatial resolution Advanced Very High Resolution Radiometer imagery (Tucker et al., 2005). All data were analyzed with consideration of first-year data as warmup.

Overall, 188 catchments were chosen according to the following criteria: (1) acceptable simulation performance, e.g., early screening NSE value of streamflow and evaporation larger than 0.6 (C. Deng, Liu, Wang, & Wang, 2018), (2) unabridged data record during the entire 21-year period, (3) relative water balance error within 10%, and (4) monthly *ET* no greater than potential *ET* (*PET*). The 188 selected catchments, which had area of 67–9806 km^2 and slope of 2.5%–25.6%, were classified into humid and (semi-)arid regions based on the *AI* (defined as the ratio of average annual *PET* to *P*) (Budyko, 1974). Catchments with $AI > 1$ were considered as (semi-)arid regions, while all others were considered as humid regions. The location and *AI* distribution of the selected catchments are shown in **Fig. 2**. The area and meteorological annual mean value of certain indices of the catchments (1983–2003) are shown in **Fig. 3**.

3.2 Parameter settings

Many previous studies have discussed the equilibrium between assimilation performance and computational demand, which is influenced by ensemble size (DeChant & Moradkhani, 2012; Evensen, 2004; Moradkhani et al., 2005). In our study, the ensemble size N was set as 1000, based on consideration of other research and the performance investigation of this study. The initial parameters and state variables were generated randomly as a Gaussian distribution, and the variance of the noise added to the parameters and the state and output variables was set on the basis of its magnitude (Leisenring & Moradkhani, 2012). The initial values of the proportionality factors were set as follows: 10% for κ and y_0 in Scheme 1; 10%, 10%, and 5% for κ, y_0, and SC in both Scheme 2 and Scheme 3; and the observation error of streamflow and evaporation was 15%. Meanwhile, the parameter variance multipliers and uncertainty bounds were used to adjust the proportion of the error automatically in Scheme 1 and Scheme 2 (Leisenring & Moradkhani, 2012). Owing to the great difficulty in applying this method in multivariate assimilation, the multipliers and uncertainty bounds were not used in Scheme 3.

4. Results and discussion

4.1 Model performance

Results of several evaluation criteria (*NSE*, *KGE*, *RMSE*, *VE*) that reflect the performance of the evapotranspiration simulation in each of the three schemes are shown in **Fig. 4**. The values of *NSE* and *KGE* in Scheme 1 and Scheme 3 (hereafter, presented as S1 and S3, respectively) are high and close to 1, while the *RMSE* value is reasonable compared with the magnitude of *ET*. Meanwhile, the values of *VE* in S1 and S3 are symmetrical on both sides of zero, and the median of which is approximate to zero. However, the relative magnitude in Scheme 2 (hereafter, presented as S2) is unacceptable. The above results demonstrate that the simulated *ET* of both S1 and S3 is plausible and that DA with the EnKF method is effective in terms of simulating *ET* well using assimilated time-varying parameters. However, the effect of S2 is unsatisfactory and its poor performance can be attributed to the lack of direct utilization of evaporation observations.

4.2 Relationships between parameters in schemes

Parameters κ and y_0 were used in all three schemes; thus, relationships between and comparisons of the two parameters among the three schemes need to be detected. Ternary diagrams reflecting the mean values of the two parameters in each of the three schemes are presented in **Fig. 5**. The mean values of κ and y_0 are nearly all situated on straight line l_2, indicating that the mean values of the two parameters assimilated from the 188 catchments under S1 and S3 are of similar order of magnitude. However, the mean values of the parameters of the catchments in S2 differ markedly from those of the other two schemes.

The correlation coefficients and diversity of the two parameters were investigated among the three schemes two by two, the results of which are drawn in half-box plots in **Fig. 6**a and **6**b. Almost all the coefficients of κ between S1 and S3 are close to 1 and the median values of y_0 are near 0.5, whereas no correlation is evident among other compared combinations. In terms of diversity, the metrics of κ

14

and y_0 are both <0.10 between S1 and S3, indicating similarity in the magnitudes of the parameters between these two schemes at each time step. Intuitively, it appears that there is a strong relationship and that κ has similar magnitude between the scheme solely using *ET* data and that using both *ET* and *Q* observations in the assimilation. Additionally, there are certain differences in the correlation coefficient in identifying y_0 after the introduction of *Q* data (i.e., S3 compared with S1).

Mutual correlation coefficients between parameters κ and y_0 in the same scheme were calculated and drawn as half-box plots in **Fig. 6**c. It can be seen that the median value of the coefficients in S1 and S2 is near zero. However, the median value of the coefficients in S3 lies near 0.6, representing clear correlation. The reason is the additional observation set in S3 (streamflow against S1; evaporation against S2) revises the model parameters better. It can activate the relationships among different climatic variables that constitute a more complete water cycle, which helps identify the relationship between two parameters.

The spatial distribution of the mean values of two parameters are drawn in Fig. S1. A similar distribution in central CONUS can be observed in relation to S1 and S3, especially for κ. There exists a type of *neighborhood effect* (i.e., similar values among neighboring catchments) in terms of the mean values of the parameters. Thus, it can be considered that the underlying surfaces and ecological attributes of these catchments are similar. In fact, these catchments are located in the same Bailey's ecoregion, which is a classification first proposed by Bailey (1994). Catchments in central CONUS belong to tropical continental and steppe regions, where similar types of natural vegetation grow. Interestingly, Carmona, Sivapalan, Yaeger, and Poveda (2014) obtained similar results using a single-parameter Budyko function. They found that catchments in the same area as identified in our study have almost the same value of parameter α.

4.3 Time series analysis of two parameters

In this section, analyses of the trend, change point, and periodicity of time-varying parameters are discussed. However, emphasis is placed on S1 and S3 owing

to the inadequate accuracy and poor performance of S2.

4.3.1 Trend analysis

As shown in **Fig. 7** and Fig. S2, there exist similar overall situations and spatial distributions of the trend of κ in S1 and S3. Decreasing and nonsignificant trends in y_0 are found in central CONUS, while increasing trends are evident in northwestern and eastern areas in S1. However, in S3, the decreasing and nonsignificant trends are retained, whereas the increasing trend in other catchments weakens. This is attributable to the introduction of streamflow data that can correct catchment attributes, especially water storage change. This aspect of this attribute is represented by y_0 (consistent with the definition by Greve et al. (2016)), which demonstrates that the method using only evaporation data cannot adequately identify the perfect trend of y_0. It should be noted that there is no obvious difference for κ.

Additional analysis was conducted in relation to other parameters and state variable S in S3, which is a comparatively more reliable scheme. Several catchments situated in central CONUS exhibit the same decreasing trend, shown by the green color in **Fig. 8**a. Similar change points detected in these catchments are also discussed in Section 4.4. Carmona et al. (2014) concluded that these central catchments (shown by the red circle in **Fig. 8**a) have similar values of parameter α (in the classical Budyko function) with abnormal runoff coefficients and evaporation ratios. Human activities have substantial impact on the MOPEX catchments in this region. Dams, surface water utilization, groundwater extraction, and changes in agricultural land are the primary factors that cause the decreasing trends and change points in this area. Moreover, such grassland regions are mostly dominated by tile and agricultural drainage (especially in Iowa, shown by the brilliant blue circle in **Fig. 8**a), which results in changes in evaporation and groundwater level. Similar attribution can be found in both Wang and Hejazi (2011) and Ye, Yaeger, Coopersmith, Cheng, and Sivapalan (2012).

4.3.2 Change point analysis

Few catchments in S1 have change points. It is noteworthy that no catchment has a change point of κ, except for two catchments in northwestern CONUS in S3, which can illustrate a weakening of change points from S1 to S3. As for y_0, change points are identified in most catchments in S1, while the number declines to 63 in S3. These catchments are scattered over CONUS, although some are distributed in the middle of the continent; detailed information is presented in Fig. S3.

Results concerning detection of the change points of state variable *storage* are shown in **Fig. 8**b. Almost the same change points are identified in central CONUS, i.e., Iowa and surrounding states. Together with the results in Section 4.3.1, it can be considered that these catchments have the same trends of decrease and similar change points of storage water (state variable in our model). Furthermore, these discoveries reflect anthropogenic influences such as the extraction and usage of groundwater and other types of water resource. Hence, the parameters identified under the finer scale in our study can be considered as indicators of these changes.

4.3.3 Periodicity analysis

The spatial distribution of periodicity in the catchments is shown in Fig. S4. The colors from green to red represent a gradual increase in the number of identified period cycles. We suppose that a period of 12 or near 12 months can represent the characteristic annual hydrological cycle, which is reasonable for catchments whose weather characteristics cycle annually. In each catchment, κ is the general parameter that might have a period of one year. Intuitively, periodicity can be deemed unreasonable when the identified period cycle is relatively long (e.g., >60 months and even up to 200 months in our identification). First, the result of S2 is considered unreasonable because the periods of κ are discrepant and far from an exact value. A period of one year can be identified in most catchments in S1 and S3, and this phenomenon is more obvious in the latter than in the former. As shown in Fig. S4d and S4f, catchments in S1 do not have periodicity in y_0, while nearly half the catchments (92 catchments) have a period of 12 months in S3. Owing to the physical significance of water storage in y_0, this can prove that additional introduction of

streamflow data can help identify the physical mechanism and definition. Catchments for which a period cannot be identified are situated in central and southwestern CONUS.

Hydrologic regions defined by the US Geological Survey are drawn in **Fig. 9**. Those catchments without periodicity (red color) are in regions 3, 5, and 10, almost consistent with the boundaries of the hydrologic regions. Catchments in region 10 are near Midwest CONUS, where human activities, especially the pattern of use of water resources, are considered the main impacts, as mentioned in Section 4.2. Catchments in regions 3 and 5 suffered vegetation reduction during 1992–2001 (Wickham, Wade, & Riitters, 2011), which might account for the lack of periodicity.

4.4 Relationships between parameters and meteorological data

Correlation coefficients between meteorological data and the parameters of corresponding months were calculated for the three schemes. Moreover, the coefficients between the parameters of corresponding months and forcing from 1–6 months prior to 1–3 months following (marked as lag-1 to lag-6 or pre-1 to pre-3) were computed to detect whether meteorological factors could impact the catchment attributes by way of delay or advance. Details of the results are illustrated in Fig. S5.

The magnitudes and situations of hysteresis in S1 and S3 are almost identical. Parameter κ has positive relationships with *ET*, *PET*, and *NDVI* and negative relationships with the difference in precipitation and evapotranspiration ($P-E$) and runoff. The absolute value of the correlation coefficient in S3 is larger than in S1, which proves that introducing streamflow data into the assimilation can slightly improve the correlation between κ and the data. Interestingly, there is certain correlation between κ and streamflow in S1, in which streamflow data were not used. The reason might be the consideration of a more complete water cycle process in calculating the other meteorological data.

Parameter y_0 has no correlation in S2 but there is weak correlation in S1

between y_0 and the meteorological data. It is noteworthy that there is positive correlation in S3 between y_0 and *ET*, *PET*, and *NDVI*, the medians of which are >0.5. Meanwhile, parameter y_0 has negative correlation with $P-E$ and R. Introducing streamflow data can activate the relationship between the assimilated parameter and other meteorological factors. The definition of y_0 is related to water available in storage, and its consideration represents a more integrated water cycle. However, its impact is indirect, because there is no obvious relationship between y_0 and storage water in S1 or S3, even if the distribution of the scatter plot data is closer in S3.

5. Conclusions

To detect rules of the intra-annual-scale variation of parameters in a changing environment, this study implemented three schemes that differed in terms of the use of observational data. Time-varying parameters of the Budyko function (evaporation calculation module) were identified using the EnKF method, and assimilated model performance assessment, correlation analysis, and time series analysis were performed. The principal conclusions derived are as follows.

(1) Plausible time-varying parameters of the Budyko function can be identified using the EnKF approach. Faithful evapotranspiration simulations of Scheme 1 (*ET* observations only) and Scheme 3 (combined *ET* and *Q* observations) can be reflected by criteria such as *NSE*, *KGE*, *RMSE*, and *VE*.

(2) Using only evaporation data in the assimilation can help identify a plausible set for parameter κ, but it is inadequate for parameter y_0 and relationships regarding meteorological data. Introducing streamflow data into the assimilation based on *ET* data can improve efficiency. More obvious periodicity of the parameters (especially y_0) can be detected. Additionally, the results obtained when using only streamflow data were unacceptable.

(3) There exist 12-month periodicities in parameters κ and y_0. Obvious trends and change points of the parameters were detected in certain regions, e.g., Midwest CONUS, as detected in previous related research. The distribution of the best estimates of parameter y_0 was found consistent with the hydrologic regions defined by the US Geological Survey. It was proved that changing conditions could be identified using the time-varying parameters of the Budyko function because of the physical significance of the parameters.

The findings imply that evaporation observations are adequate when comparing simple catchment attributes. However, streamflow observations are also necessary when focusing on additional processes such as soil water content. Further research should focus on attributing physical mechanisms to the parameters and applying these relationships to predictions.

Acknowledgments

This study was supported by the Joint Funds of the National Natural Science Foundation of China (Grant No. U1865201), National Natural Science Foundation of China (Grant No. 51861125102), and Innovation Team in Key Field of the Ministry of Science and Technology (grant no. 2018RA4014).

Code/ Data availability

Precipitation and streamflow data were obtained from the Model Parameter Estimation Experiment dataset (Duan et al., 2006), and potential evaporation and actual evaporation data were collected from (K. Zhang et al., 2010). Other data, models, or code used in the study are available from the corresponding author upon reasonable request.

References

Abbaszadeh, P., Moradkhani, H., & Yan, H. X. (2018). Enhancing hydrologic data assimilation by evolutionary Particle Filter and Markov Chain Monte Carlo. *Advances in Water Resources, 111*, 192-204. doi:https://doi.org/10.1016/j.advwatres.2017.11.011

Bagrov, N. A. (1953). On multi-year average of evapotranspiration from land surface. *Met. Gidrol., (10)*, 20-25.

Bailey, R. G., P. E. Avers, T. King, and W. H. McNab (Eds.). (1994). Ecoregions and subregions of the United States, with supplementary table of map unit descriptions, scale 1:7,500,000. *USDA For. Serv.*, Washington, D. C. [Map].

Budyko, M. I. (1974). Climate and Life. *Academic, New York*.

Carmona, A. M., Sivapalan, M., Yaeger, M. A., & Poveda, G. (2014). Regional patterns of interannual variability of catchment water balances across the continental US: A Budyko framework. *Water Resources Research, 50*(12), 9177-9193. doi:https://doi.org/10.1002/2014WR016013

Clark, M. P., Rupp, D. E., Woods, R. A., Zheng, X., Ibbitt, R. P., Slater, A. G., . . . Uddstrom, M. J. (2008). Hydrological data assimilation with the ensemble Kalman filter: Use of streamflow observations to update states in a distributed hydrological model. *Advances in Water Resources, 31*(10), 1309-1324. doi:https://doi.org/10.1016/j.advwatres.2008.06.005

de Vos, N. J., Rientjes, T. H. M., & Gupta, H. V. (2010). Diagnostic evaluation of conceptual rainfall-runoff models using temporal clustering. *Hydrological Processes, 24*(20), 2840-2850. doi:https://doi.org/10.1002/hyp.7698

DeChant, C. M., & Moradkhani, H. (2012). Examining the effectiveness and robustness of sequential data assimilation methods for quantification of uncertainty in hydrologic forecasting. *Water Resources Research, 48*. doi:https://doi.org/10.1029/2011WR011011

Deng, C., Liu, P., Guo, S., Li, Z., & Wang, D. (2016). Identification of hydrological model parameter variation using ensemble Kalman filter. *Hydrology and Earth System Sciences, 20*(12), 4949-4961. doi:10.5194/hess-20-4949-2016

Deng, C., Liu, P., Guo, S. L., Wang, H., & Wang, D. B. (2015). Estimation of nonfluctuating reservoir inflow from water level observations using methods based on flow continuity. *Journal of Hydrology, 529*, 1198-1210. doi:https://doi.org/10.1016/j.jhydrol.2015.09.037

Deng, C., Liu, P., Wang, D. B., & Wang, W. G. (2018). Temporal variation and scaling of parameters for a monthly hydrologic model. *Journal of Hydrology, 558*, 290-300. doi:https://doi.org/10.1016/j.jhydrol.2018.01.049

Duan, Q., Schaake, J., Andreassian, V., Franks, S., Goteti, G., Gupta, H. V., . . . Wood, E. F. (2006). Model Parameter Estimation Experiment (MOPEX): An overview of science strategy and major results from the second and third workshops. *Journal of Hydrology, 320*(1-2), 3-17. doi:https://doi.org/10.1016/j.jhydrol.2005.07.031

Evensen, G. (1994). Sequential Data Assimilation with a Nonlinear Quasi-Geostrophic Model Using Monte-Carlo Methods To Forecast Error Statistics. *Journal of Geophysical Research-Oceans, 99*(C5), 10143-10162. doi:https://doi.org/10.1029/94JC00572

Evensen, G. (2004). Sampling strategies and square root analysis schemes for the EnKF. *Ocean Dynamics, 54*(6), 539-560. doi:https://doi.org/10.1007/s10236-004-0099-2

Feng, M. Y., Liu, P., Guo, S. L., Shi, L. S., Deng, C., & Ming, B. (2017). Deriving adaptive operating rules of hydropower reservoirs using time-varying parameters generated by the EnKF. *Water Resources Research, 53*(8), 6885-6907. doi:https://doi.org/10.1002/2016WR020180

Fu, B. P. (1981). On the calculation of the evaporation from land surface [in Chinese]. *Sci. Atmos., 5(1)*, 23-31.
Greve, P., Gudmundsson, L., Orlowsky, B., & Seneviratne, S. I. (2016). A two-parameter Budyko function to represent conditions under which evapotranspiration exceeds precipitation. *Hydrology and Earth System Sciences, 20*(6), 2195-2205. doi:https://doi.org/10.5194/hess-20-2195-2016
Jeremiah, E., Marshall, L., Sisson, S. A., & Sharma, A. (2013). Specifying a hierarchical mixture of experts for hydrologic modeling: Gating function variable selection. *Water Resources Research, 49*(5), 2926-2939. doi:https://doi.org/10.1002/wrcr.20150
Kendall, M. G. (1975). Rank Correlation Methods. . *4th Edition, Charles Griffin, London.*
Leisenring, M., & Moradkhani, H. (2012). Analyzing the uncertainty of suspended sediment load prediction using sequential data assimilation. *Journal of Hydrology, 468*, 268-282. doi:https://doi.org/10.1016/j.jhydrol.2012.08.049
Mann, H. B. (1945). Nonparametric Tests against Trend. *Econometrica, 13*, 245-259. doi:https://doi.org/10.2307/1907187
Marshall, L., Sharma, A., & Nott, D. (2006). Modeling the catchment via mixtures: Issues of model specification and validation. *Water Resources Research, 42*(11). doi:https://doi.org/10.1029/2005WR004613
Merz, R., Parajka, J., & Bloschl, G. (2011). Time stability of catchment model parameters: Implications for climate impact analyses. *Water Resources Research, 47*. doi:https://doi.org/10.1029/2010WR009505
Mezentsev, V. S. (1955). More on the calculation of average total evaporation. *Met. Gidrol., 5*, 24-26.
Mianabadi, A., Davary, K., Pourreza-Bilondi, M., & Coenders-Gerrits, A. M. J. (2020). Budyko framework; towards non-steady state conditions. *Journal of Hydrology, 588*. doi:https://doi.org/10.1016/j.jhydrol.2020.125089
Milly, P. C. D. (1994). Climate, Soil-Water Storage, and the Average Annual Water-Balance. *Water Resources Research, 30*(7), 2143-2156. doi:https://doi.org/10.1029/94WR00586
Mitchell, H. L., & Houtekamer, P. L. (2000). An adaptive ensemble Kalman filter. *Monthly Weather Review, 128*(2), 416-433. doi:https://doi.org/10.1175/1520-0493(2000)128<0416:AAEKF>2.0.CO;2
Monteith, J. L. (1972). Solar radiation and productivity in tropical ecosystem. *J. Appl. Ecol., 9*, 747-766.
Moradkhani, H., Sorooshian, S., Gupta, H. V., & Houser, P. R. (2005). Dual state-parameter estimation of hydrological models using ensemble Kalman filter. *Advances in Water Resources, 28*(2), 135-147. doi:https://doi.org/10.1016/j.advwatres.2004.09.002
Nash, J. E., & Sutcliffe, J. V. (1970). River flow forecasting through conceptual models Part I-a discussion of princi-ples. *Journal of Hydrology, 10*, 282-290. doi:https://doi.org/10.1016/0022-1694(70)90255-6
Patil, S. D., & Stieglitz, M. (2015). Comparing Spatial and temporal transferability of hydrological model parameters. *Journal of Hydrology, 525*, 409-417. doi:https://doi.org/10.1016/j.jhydrol.2015.04.003
Peel, M. C., & Bloschl, G. (2011). Hydrological modelling in a changing world. *Progress in Physical Geography-Earth and Environment, 35*(2), 249-261. doi:https://doi.org/10.1177/0309133311402550
Penman, H. L. (1948). Natural evaporation from open water, bare and grass. *Proc. R. Soc., 193*, 120-145.
Pettitt, A. N. (1979). A Non-Parametric Approach to the Change-Point Problem. *Applied Statistics, 28*, 126-135. doi:https://doi.org/10.2307/2346729
Pike, J. G. (1964). The estimation of annual run-off from meteorological data in a tropical climate. *2*(2), 116-123. doi:https://doi.org/10.1016/0022-1694(64)90022-8
Porporato, A., Daly, E., & Rodriguez-Iturbe, I. (2004). Soil water balance and

ecosystem response to climate change. *American Naturalist, 164*(5), 625-632. doi:https://doi.org/10.1086/424970

Priestley, C. H. B. a. T., R.J. (1972). On the Assessment of Surface Heat Flux and Evaporation Using Large-Scale Parameters. *Monthly Weather Review, 100*, 81-82. doi:https://doi.org/10.1175/1520-0493(1972)100<0081:OTAOSH>2.3.CO;2

Sankarasubramanian., A., Wang, D., Archfield, S., Reitz, M., Vogel, R. M., Mazrooei, A., & Mukhopadhyay, S. (2020). HESS Opinions: Beyond the long-term water balance: evolving Budyko's supply–demand framework for the Anthropocene towards a global synthesis of land-surface fluxes under natural and human-altered watersheds. *Hydrology and Earth System Sciences, 24*(4), 1975-1984. doi:10.5194/hess-24-1975-2020

Seibert, J., McDonnell, J. J., & Woodsmith, R. D. (2010). Effects of wildfire on catchment runoff response: a modelling approach to detect changes in snow-dominated forested catchments. *Hydrology Research, 41*(5), 378-390. doi:https://doi.org/10.2166/nh.2010.036

Shao Xiaomei, X. Y., Yan Changrong. (2006). Wavelet Analysis of Rainfall Variation in the Yellow River Basin (in Chinese). . *Acta Scientiarum Naturalium Universitatis Pekinensis, 42*(No.4).

Sinha, J., Jha, S., & Goyal, M. K. (2019). Influences of watershed characteristics on long-term annual and intra-annual water balances over India. *Journal of Hydrology, 577*. doi:https://doi.org/10.1016/j.jhydrol.2019.123970

Smith, P. J., Beven, K. J., & Tawn, J. A. (2008). Detection of structural inadequacy in process-based hydrological models: A particle-filtering approach. *Water Resources Research, 44*(1). doi:https://doi.org/10.1029/2006WR005205

Snyder, C., & Zhang, F. Q. (2003). Assimilation of simulated Doppler radar observations with an ensemble Kalman filter. *Monthly Weather Review, 131*(8), 1663-1677. doi:https://doi.org/10.1175//2555.1

Thirel, G., Andreassian, V., Perrin, C., Audouy, J. N., Berthet, L., Edwards, P., . . . Vaze, J. (2015). Hydrology under change: an evaluation protocol to investigate how hydrological models deal with changing catchments. *Hydrological Sciences Journal-Journal Des Sciences Hydrologiques, 60*(7-8), 1184-1199. doi:https://doi.org/10.1080/02626667.2014.967248

Tucker, C. J., Pinzon, J. E., Brown, M. E., Slayback, D. A., Pak, E. W., Mahoney, R., . . . El Saleous, N. (2005). An extended AVHRR 8-km NDVI dataset compatible with MODIS and SPOT vegetation NDVI data. *International Journal of Remote Sensing, 26*(20), 4485-4498. doi:https://doi.org/10.1080/01431160500168686

Turc, L. (1954). Le bilan d'eau des sols: Relation entre la précipitation, l'évaporation et l'écoulement. *Ann. Agron., 5*, 491-569.

Vaze, J., Post, D. A., Chiew, F. H. S., Perraud, J. M., Viney, N. R., & Teng, J. (2010). Climate non-stationarity - Validity of calibrated rainfall-runoff models for use in climate change studies. *Journal of Hydrology, 394*(3-4), 447-457. doi:https://doi.org/10.1016/j.jhydrol.2010.09.018

Vrugt, J. A., ter Braak, C. J. F., Diks, C. G. H., & Schoups, G. (2013). Hydrologic data assimilation using particle Markov chain Monte Carlo simulation: Theory, concepts and applications. *Advances in Water Resources, 51*, 457-478. doi:https://doi.org/10.1016/j.advwatres.2012.04.002

Wang, D. B., & Hejazi, M. (2011). Quantifying the relative contribution of the climate and direct human impacts on mean annual streamflow in the contiguous United States. *Water Resources Research, 47*. doi:https://doi.org/10.1029/2010WR010283

Westra, S., Thyer, M., Leonard, M., Kavetski, D., & Lambert, M. (2014). A strategy for diagnosing and interpreting hydrological model nonstationarity. *Water Resources Research, 50*(6), 5090-5113. doi:https://doi.org/10.1002/2013WR014719

Wickham, J. D., Wade, T. G., & Riitters, K. H. (2011). An environmental assessment

of United States drinking water watersheds. *Landscape Ecology, 26*(5), 605-616. doi:https://doi.org/10.1007/s10980-011-9591-5

Wu, K. S., & Johnston, C. A. (2007). Hydrologic response to climatic variability in a Great Lakes Watershed: A case study with the SWAT model. *Journal of Hydrology, 337*(1-2), 187-199. doi:https://doi.org/10.1016/j.jhydrol.2007.01.030

Xiong, L. H., & Guo, S. L. (1999). A two-parameter monthly water balance model and its application. *Journal of Hydrology, 216*(1-2), 111-123. doi:https://doi.org/10.1016/S0022-1694(98)00297-2

Xiong, M. S., Liu, P., Cheng, L., Deng, C., Gui, Z. L., Zhang, X. J., & Liu, Y. H. (2019). Identifying time-varying hydrological model parameters to improve simulation efficiency by the ensemble Kalman filter: A joint assimilation of streamflow and actual evapotranspiration. *Journal of Hydrology, 568*, 758-768. doi:https://doi.org/10.1016/j.jhydrol.2018.11.038

Yang, D. W., Sun, F. B., Liu, Z. Y., Cong, Z. T., Ni, G. H., & Lei, Z. D. (2007). Analyzing spatial and temporal variability of annual water-energy balance in nonhumid regions of China using the Budyko hypothesis. *Water Resources Research, 43*(4). doi:https://doi.org/10.1029/2006WR005224

Ye, S., Yaeger, M., Coopersmith, E., Cheng, L., & Sivapalan, M. (2012). Exploring the physical controls of regional patterns of flow duration curves - Part 2: Role of seasonality, the regime curve, and associated process controls. *Hydrology and Earth System Sciences, 16*(11), 4447-4465. doi:https://doi.org/10.5194/hess-16-4447-2012

Zhang, K., Kimball, J. S., Nemani, R. R., & Running, S. W. (2010). A continuous satellite-derived global record of land surface evapotranspiration from 1983 to 2006. *Water Resources Research, 46*. doi:https://doi.org/10.1029/2009WR008800

Zhang, L., Dawes, W. R., & Walker, G. R. (2001). Response of mean annual evapotranspiration to vegetation changes at catchment scale. *Water Resources Research, 37*(3), 701-708. doi: https://doi.org/10.1029/2000WR900325

Zhang, L., Hickel, K., Dawes, W. R., Chiew, F. H. S., Western, A. W., & Briggs, P. R. (2004). A rational function approach for estimating mean annual evapotranspiration. *Water Resources Research, 40*(2). doi:https://doi.org/10.1029/2003WR002710

Zhang, X., Dong, Q., Cheng, L., & Xia, J. (2019). A Budyko-based framework for quantifying the impacts of aridity index and other factors on annual runoff. *Journal of Hydrology, 579*. doi:10.1016/j.jhydrol.2019.124224

Ziegler, A. D., Sheffield, J., Maurer, E. P., Nijssen, B., Wood, E. F., & Lettenmaier, D. P. L. (2003). Detection of intensification in global- and continental-scale hydrological cycles: Temporal scale of evaluation. *Journal of Climate, 16*(3), 535-547. doi:https://doi.org/10.1175/1520-0442(2003)016<0535:DOIIGA>2.0.CO;2

24

List of tables

25

720 **Table 1.** Descriptions and ranges of parameters set in this study.

Parameters	Description	Interval and unit
κ	Watershed parameter	1.0-4.0 (-)
y_0	Evaporation/storage parameter	0.1-0.7 (-)
SC	Water storage capacity	100-2000 (mm)

721

722

26

723 **Table 2.** Descriptions of the assimilated time-varying parameters, calculation modules
724 and observational data of the designed experimental schemes.

Schemes	Description
Scheme 1	Only use two-parameter Budyko model, P, PET, ***ET*** data for DA
Scheme 2	Use two-parameter Budyko model together with monthly runoff calculation, P, PET, ***Q*** data for DA
Scheme 3	Use two-parameter Budyko model together with monthly runoff calculation, P, PET, ***Q and ET*** data for DA

725

27

List of figures

28

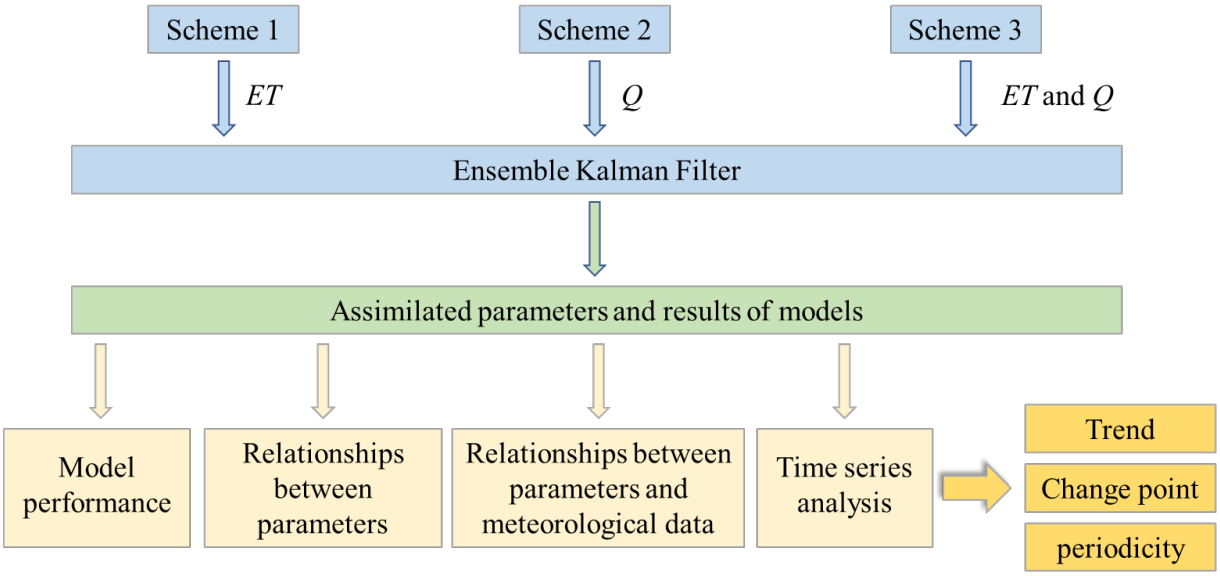

745 **Fig. 1** Framework of the methodologies used and corresponding experimental design
746 together with the structure of the analysis adopted in this paper. *ET* and *Q* next to the
747 first row of arrows represent utilized observational data in Ensemble Kalman Filter
748 (*ET*: evapotranspiration, *Q*: streamflow).

749

29

750 **Fig. 2** Locations of the 188 selected catchments and the corresponding aridity index
751 (*AI*) of humid catchments (blue) and (semi-)arid catchments (pale yellow).

752

30

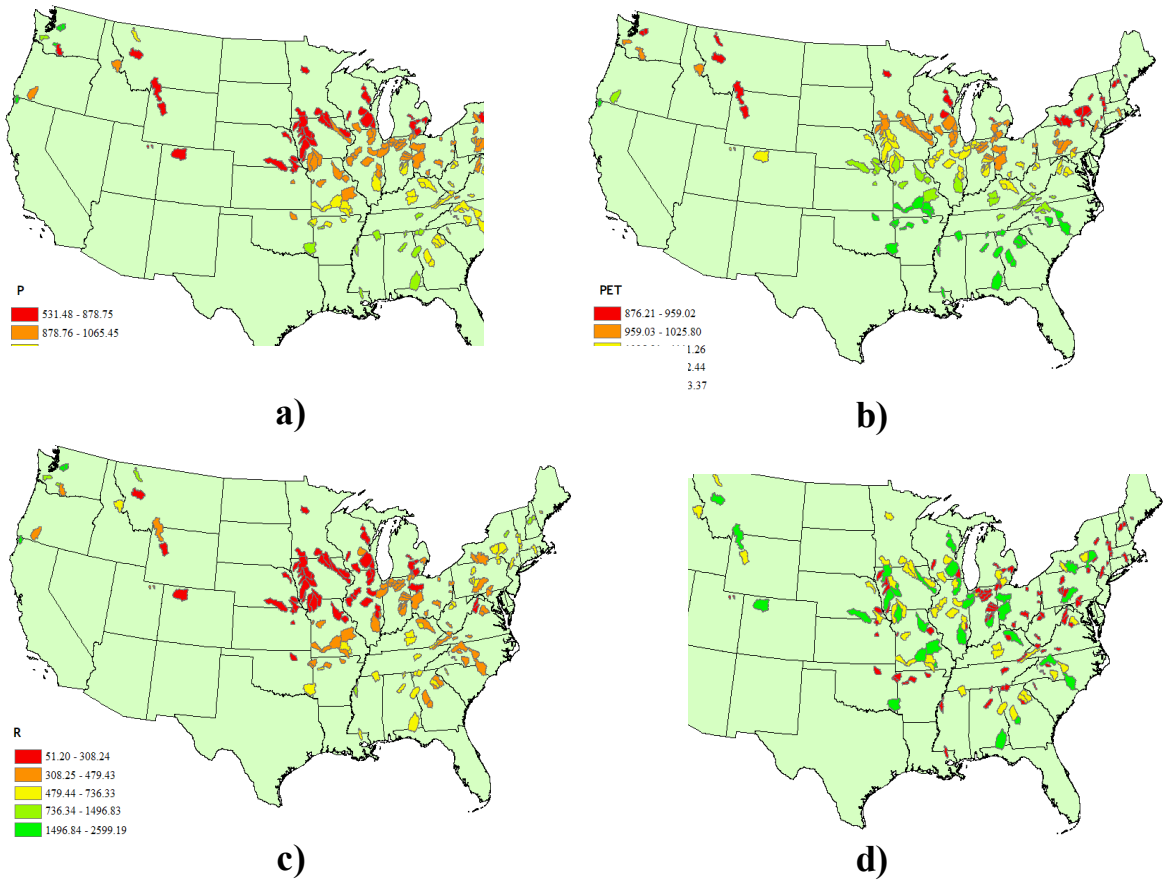

753

754 **Fig. 3** Annual mean values of meteorological variables: **a)** precipitation, **b)** potential
755 evapotranspiration, and **c)** runoff and **d)** the area of the 188 selected catchments.

756

31

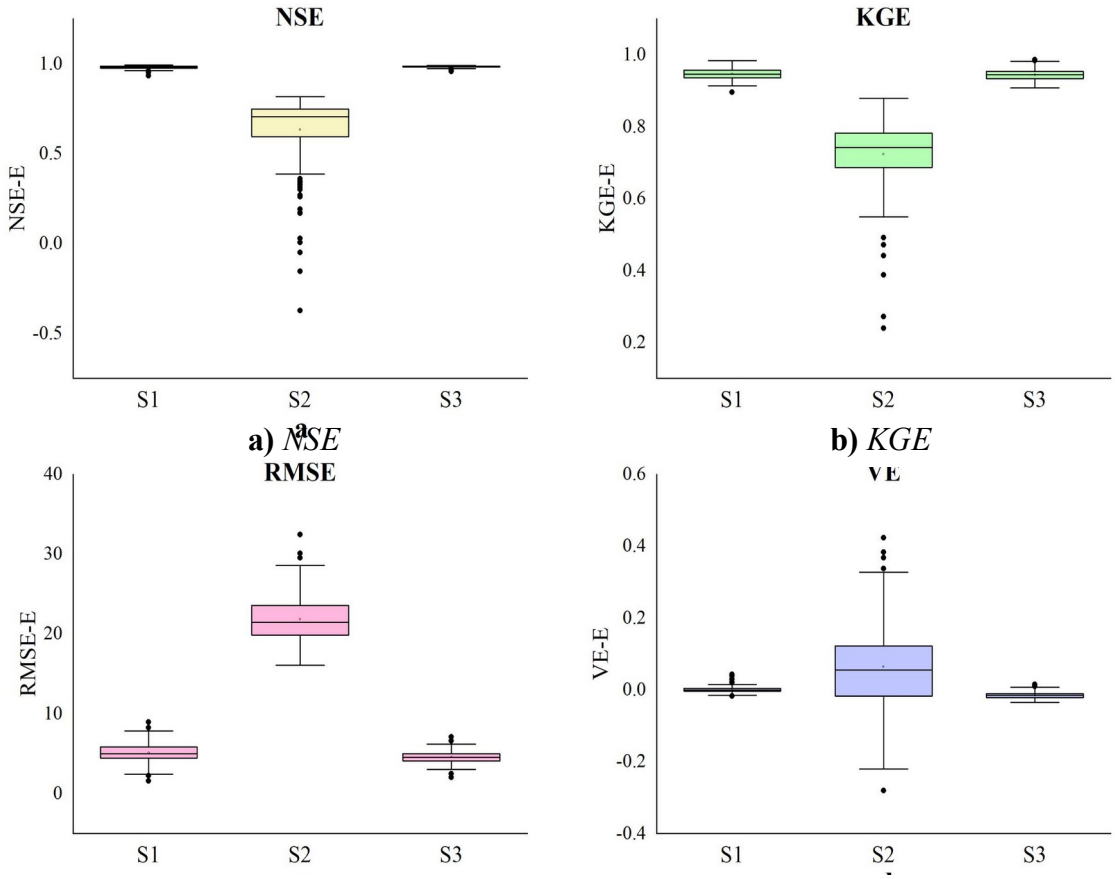

a) *NSE* **b)** *KGE* **c)** *RMSE* **d)** *VE*

Fig. 4 Box figures of four evaluation criteria **a)** *NSE* **b)** *KGE* **c)** *RMSE* **d)** *VE* of *ET* simulations in the three schemes. In the plots, the whiskers represent the minimum and maximum values, the bottom and top of the boxes are the 25th and 75th percentiles, respectively, and the horizontal lines are the median values.

32

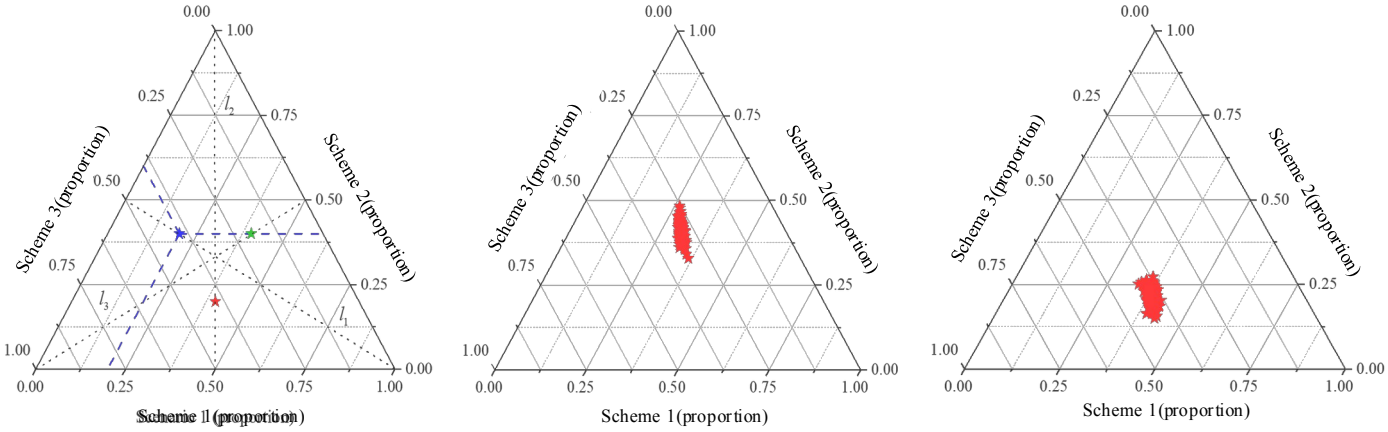

762 **Fig. 5** Ternary diagrams of the mean values of the parameters in the three schemes. **a)**
763 Example in which the three stars represent three sets of data (each having three
764 proportions of the parameter values). The proportions were calculated based on the
765 ratio of the value in the corresponding scheme to the sum of the values in the three
766 schemes. Line l_1 indicates points at which the location of the blue star has the same
767 proportion in S2 and S3, line l_2 is the same for S1 and S3, and line l_3 corresponds to
768 S1 and S2. **b)** and **c)** the distribution of magnitude of κ and y_0, respectively, where
769 the stars are situated on line l_2.
770

33

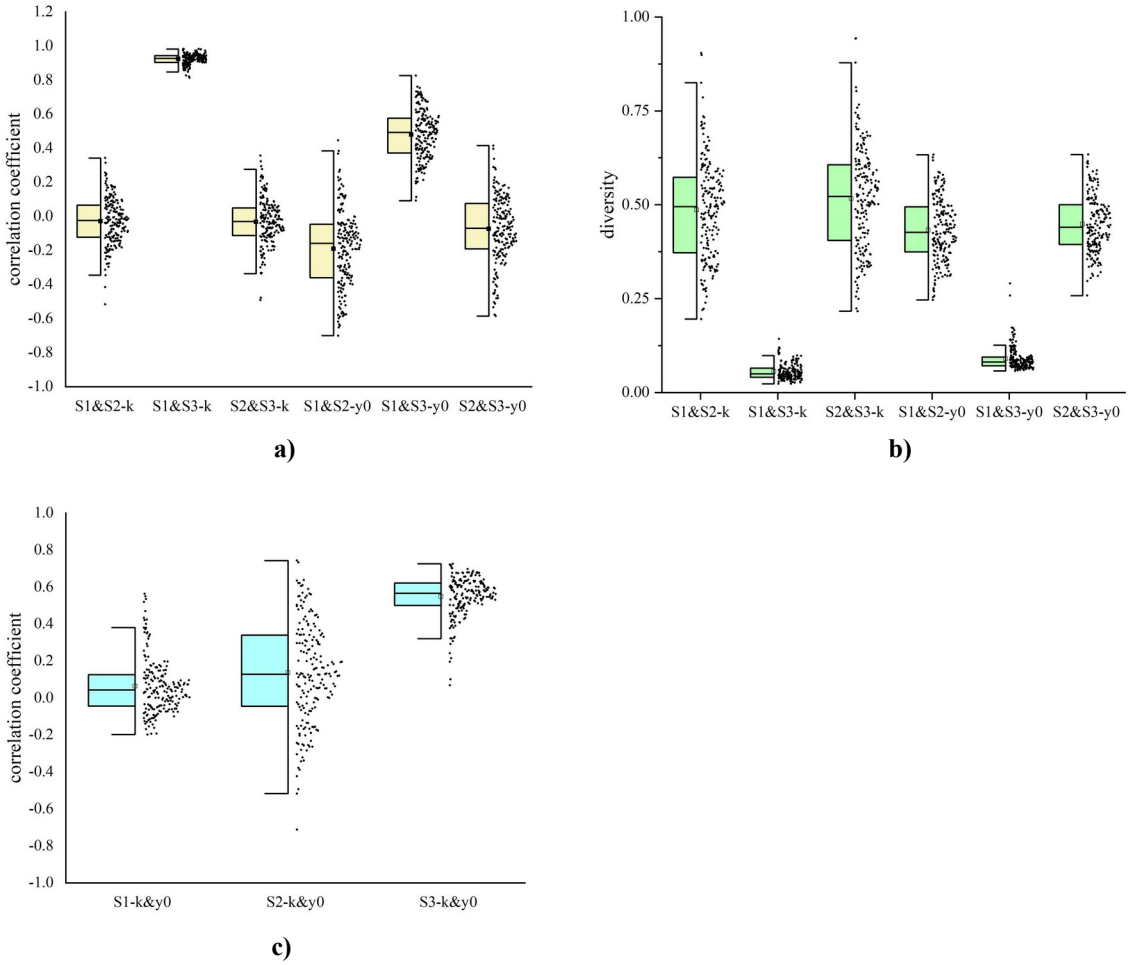

771 **Fig. 6** Half-box plots of the correlation coefficients of **a)** κ and **b)** y_0 between the
772 different schemes two by two, and **c)** half-box diagram of correlation between κ and
773 y_0 in each scheme. In the plots, the whiskers represent the minimum and maximum
774 values, the bottom and top of the boxes are the 25th and 75th percentiles, respectively,
775 and the horizontal lines are the median values. The data scatter plot forms the right
776 side of the half-box.

777

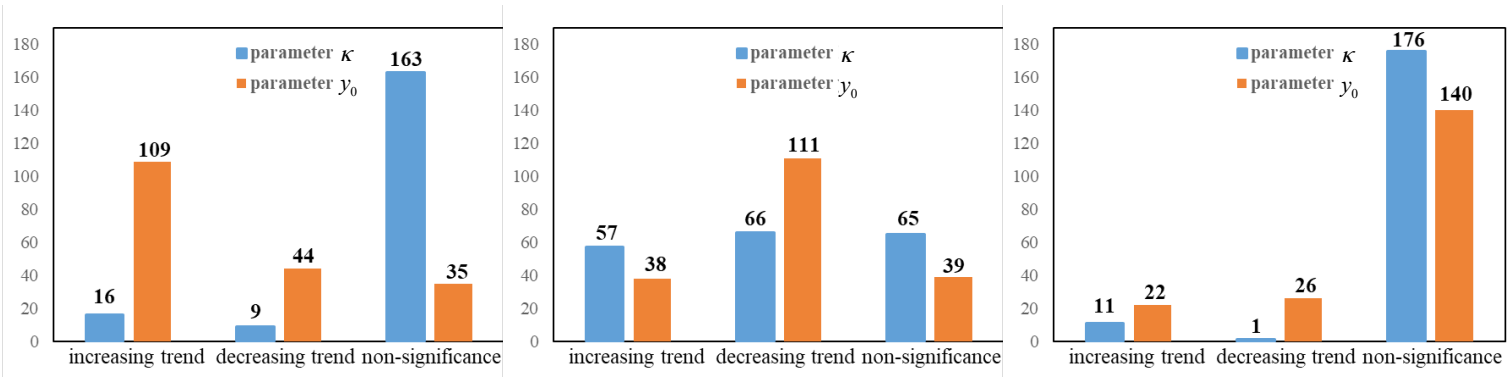

778 **Fig. 7** Number of catchments with increasing, decreasing, and nonsignificant trends of

779 the parameters (κ and y_0) in **a)** S1, **b)** S2, and **c)** S3.

780

35

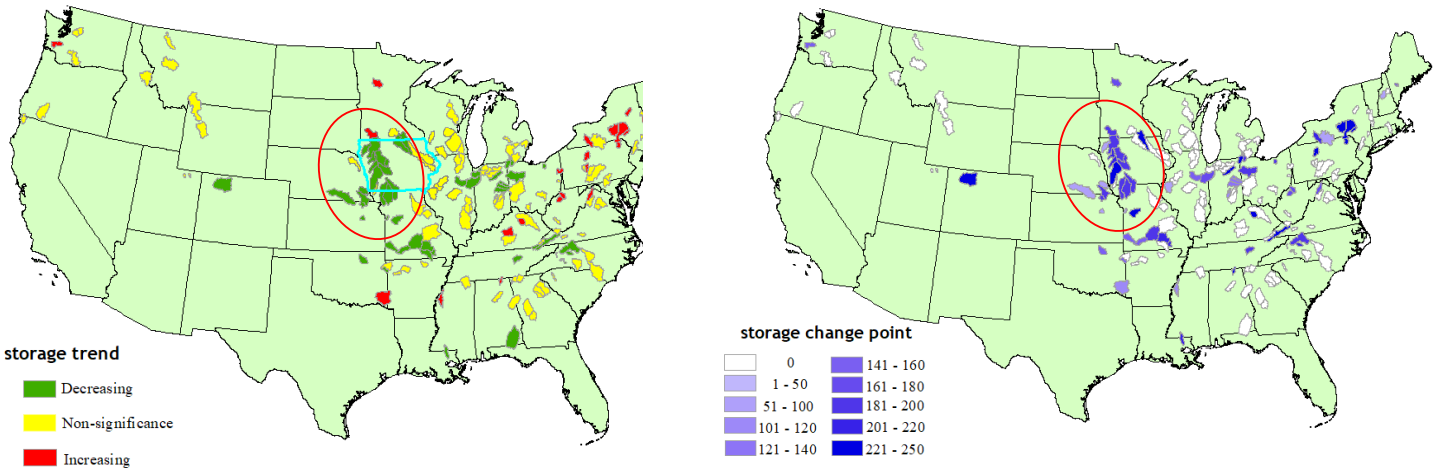

a) **b)**

781 **Fig. 8** Spatial distribution of **a)** trend and **b)** change point conditions of state variable
782 *storage* in Scheme 3.

783

36

18

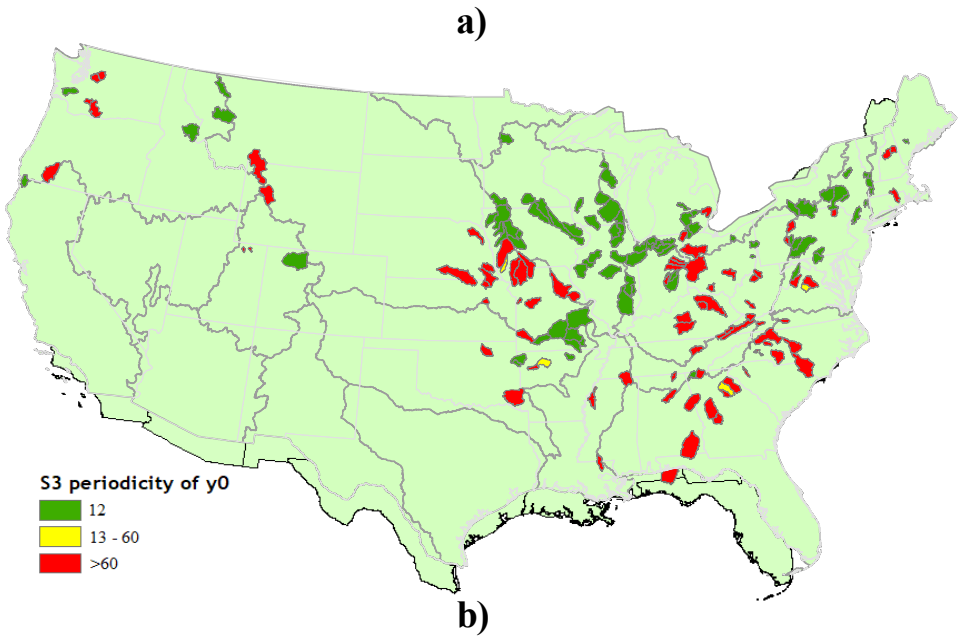

784

785 **Fig. 9 a)** US Geological Survey hydrologic regions with state boundaries where the

786 number of each region is revealed. **b)** Periodicity of y_0 in Scheme 3, where
787 catchments colored green represent a period of 12 months, and the others generally
788 represent no period.

789

37

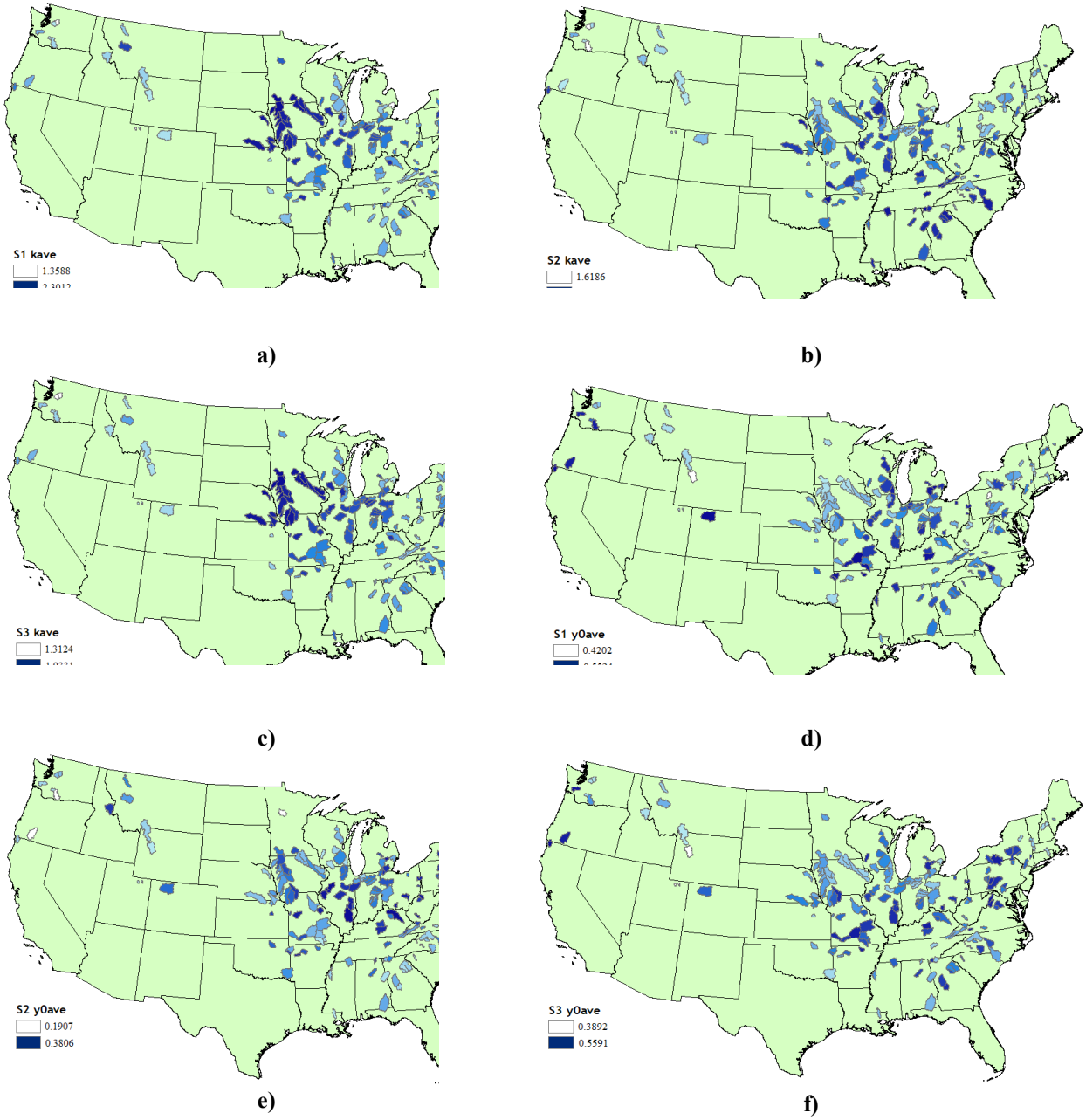

790 **Fig. S1** Spatial distribution of mean values of parameters: **a) – c)** κ and **d) – f)** y_0.
791 **a)** and **d)** represent S1, **b)** and **e)** represent S2, and **c)** and **f)** represent S3. Color
792 intensity indicates the magnitude of the parameter value. Accordingly, catchments
793 with similar color have similar parameter values.

794

795

38

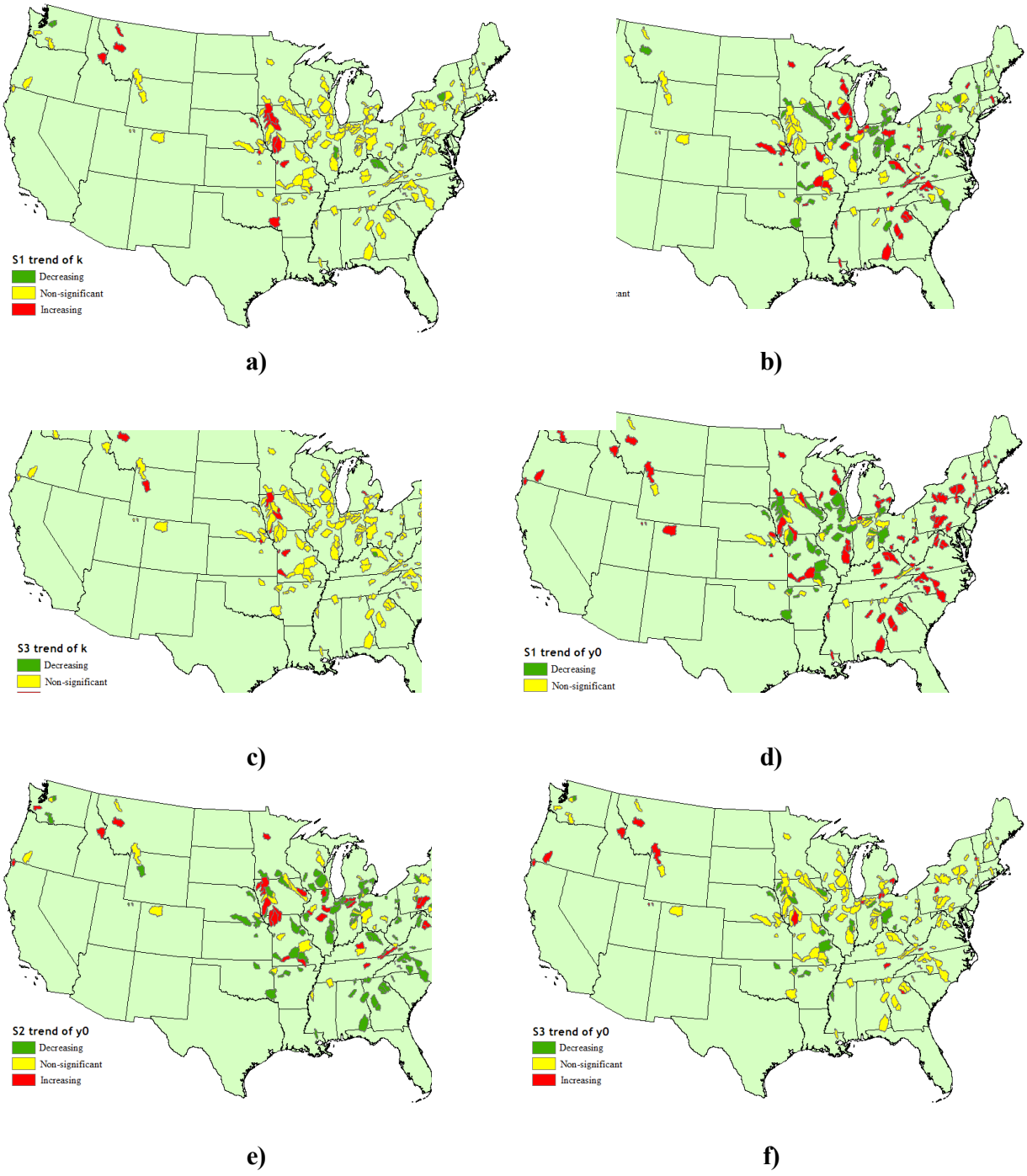

796 **Fig. S2** Spatial distribution of trends of parameters: **a) – c)** κ and **d) – f)** y_0. **a)** and
797 **d)** represent S1, **b)** and **e)** represent S2, and **c)** and **f)** represent S3. Red indicates an
798 increasing trend, green means a decreasing trend, and yellow represents a
799 nonsignificant result of the trend analysis.

800

39

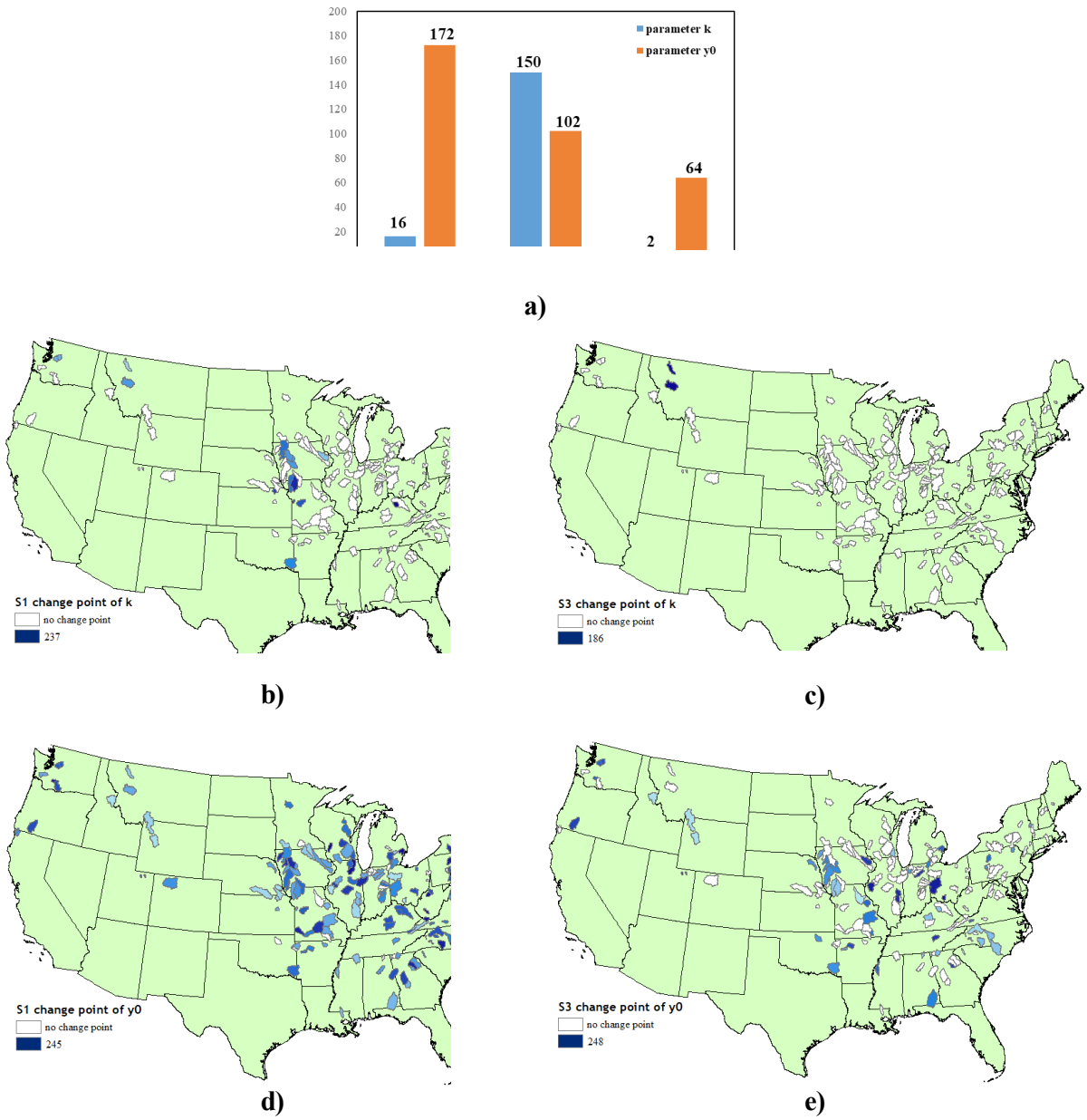

801 **Fig. S3** Overall number of change points of **a)** the two parameters, **b)** and **c)** k, and

802 **d)** and **e)** y_0. Color intensity represents the magnitude of the time step; a darker color

803 indicates a greater number of change points with a large time step.

804

40

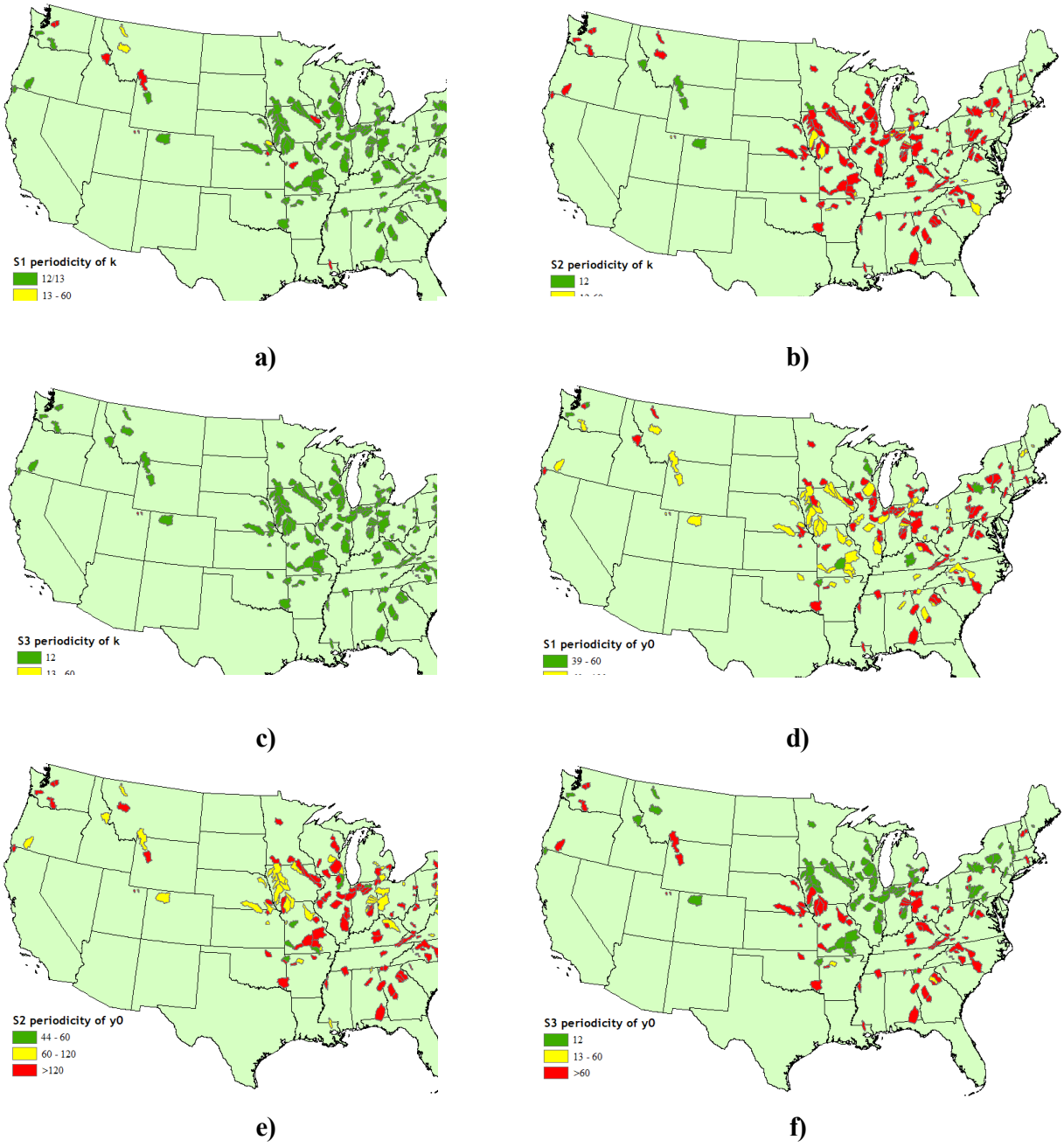

805 **Fig. S4** Spatial distribution of the periodicity identified in the parameters: **a)** – **c)** K

806 and **d)** – **f)** y_0. **a)** and **d)** represent S1, **b)** and **e)** represent S2, and **c)** and **f)** represent
807 S3. Colors of catchments indicate different periodicity corresponding to the legend at
808 the bottom left of each panel.

809

41

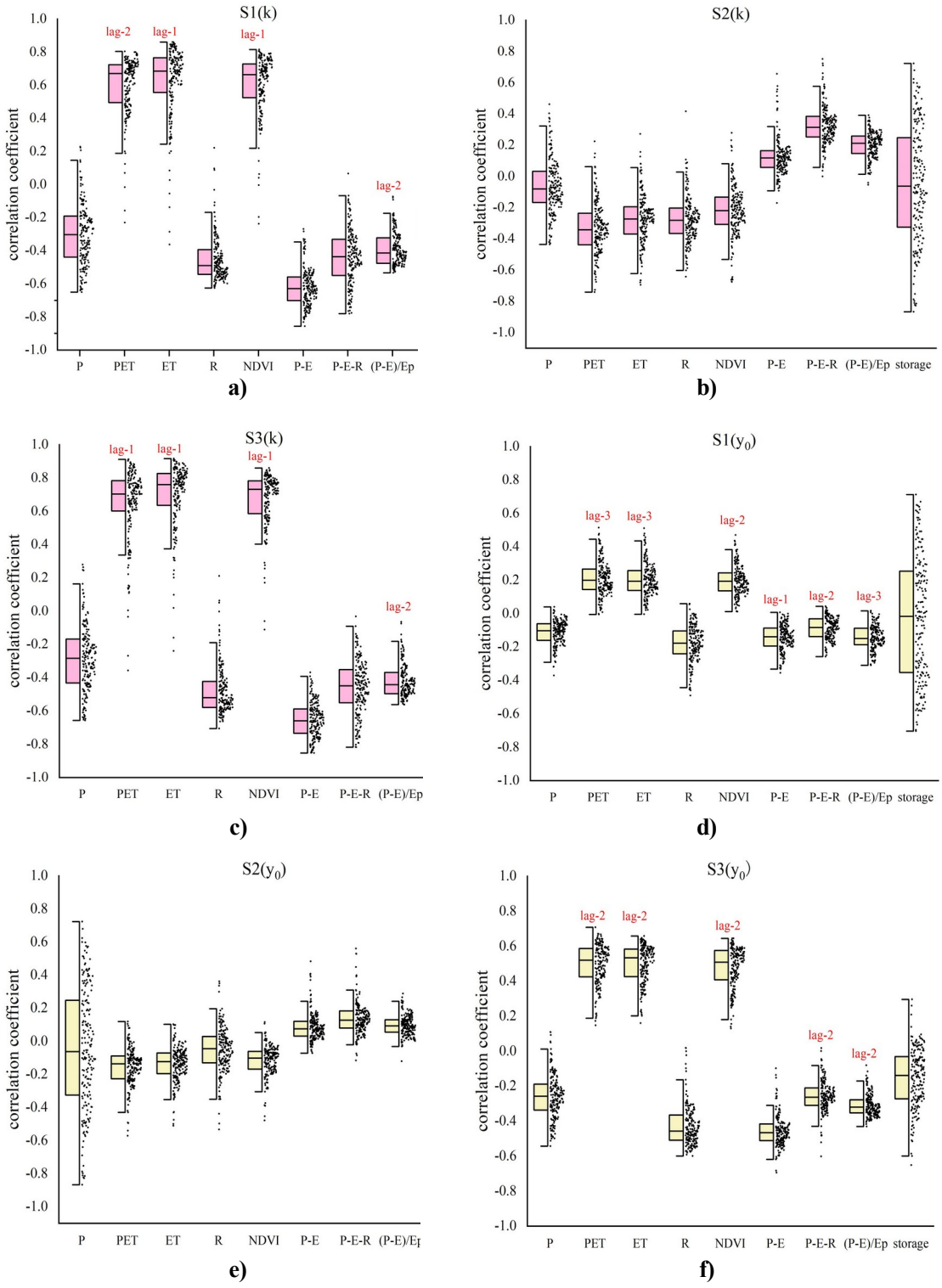

Fig. S5 Half-box plots of the correlation coefficient between meteorological data and parameters κ and y_0 in **a)** and **d)** S1, **b)** and **e)** S2, and **c)** and **f)** S3. Red labels represent the lag-1 to lag-6 and pre-1 to pre-3 mentioned in Section 4.4.

42